

Structure and optical properties of $\text{Li}_2\text{Ga}_2\text{GeS}_6$ nonlinear crystal



L.I. Isaenko^{a,b}, A.P. Yelissev^{a,*}, S.I. Lobanov^a, P.G. Krinitin^a, M.S. Molokev^{c,d}

^a V.S. Sobolev Institute of Geology and Mineralogy SB RAS, Novosibirsk 630090, Russia

^b Novosibirsk State University, 2 Pirogova Street, Novosibirsk 630090, Russia

^c L.V. Kirensky Institute of Physics SB RAS, Krasnoyarsk 660036, Russia

^d Far Eastern State Transport University, Khabarovsk 680021, Russia

ARTICLE INFO

Article history:

Received 8 May 2015

Accepted 6 June 2015

Available online 11 June 2015

Keywords:

$\text{Li}_2\text{Ga}_2\text{GeS}_6$

Structure

Absorption

Raman

Luminescence

Excitons

ABSTRACT

Structure and optical properties of new nonlinear crystal – $\text{Li}_2\text{Ga}_2\text{GeS}_6$ single crystal of optical quality, grown by the Bridgman technique were studied. The data on transmission, Raman scattering, luminescence emission, excitation and thermal quenching as well as thermostimulated luminescence are presented. Fundamental absorption edge is determined by the direct allowed electronic transitions: The values of optical band gap are estimated. Absorption band at $8.0 \mu\text{m}$ is due to S–S vibrations. Features in photoluminescence spectra are associated with excitons: both free (narrow line at 371 nm) and self-trapped ones (broad bands at 596 , 730 and 906 nm). Spontaneous emission in the 80 – 170 K range, both at crystal heating and cooling, is typical of pyroelectrics: This confirms the absence of symmetry center in $\text{Li}_2\text{Ga}_2\text{GeS}_6$ and an opportunity of laser frequency nonlinear conversion.

© 2015 Elsevier B.V. All rights reserved.

1. Introduction

Optical parametric oscillation (OPO) is today one of the most widespread ways to produce tunable coherent radiation. The main part of OPO is a nonlinear crystal. The most widely used nonlinear crystals for the mid-IR are silver thiogallate and selenogallates (AgGaS_2 and AgGaSe_2) [1,2], zinc germanium phosphide ZnGeP_2 [3], etc.: these crystals have been practically used IR NLO materials since the 1970s. However, they possess serious drawbacks of one or another in their properties. For example, AgGaS_2 and AgGaSe_2 have a low laser-damage threshold, AgGaSe_2 is not phase-matchable at $1 \mu\text{m}$ (Nd:YAG), and ZnGeP_2 exhibits strong two-photon absorption of conventional $1 \mu\text{m}$ (Nd:YAG) or $1.55 \mu\text{m}$ (Yb:YAG) laser-pumping sources.

Two ways are used to overcome these drawbacks. One way is to synthesize a quaternary compound which is formed by the solid solution between the parent AgGaS_2 and GeS_2 . The improved laser damage threshold of AgGaGeS_4 made it a promising alternative to the widely used AgGaS_2 for a frequency down-converter with a Nd:YAG laser pumping as well as for many other applications [4–6]. Another way is to obtain crystals of the LiBC_2 family, where $B = \text{In}$, Ga and $C = \text{S}$, Se , Te : these crystals have large band gap up to 4 eV . As a result their optical damage thresholds exceed the parameters of their Ag-containing analogues although nonlinear susceptibility of Li-compounds is somewhat lower [7–9]. During

last years one tries to combine these approaches and to create a quaternary compound based both on LiGaS_2 and GeS_2 . Thus in [10] authors synthesized a fine grained powder of $\text{Li}_2\text{Ga}_2\text{GeS}_6$ and its structure was established as orthorhombic. These authors recorded also the transmission spectra of this powder mixed with KBr and estimated its nonlinear susceptibility as 16 pm/V which is comparable with that for AgGaS_2 (19 pm/V) and AgGaGeS_4 (15 pm/V) [10]. It is important that 1. nonlinear susceptibility of $\text{Li}_2\text{Ga}_2\text{GeS}_6$ is considerably higher in comparison with LiGaS_2 which has $d_{31} = 5.8 \text{ pm/V}$ [11] and 2. $\text{Li}_2\text{Ga}_2\text{GeS}_6$ is considerably more stable under the pumping from the Nd-YAG laser in comparison with AgGaS_2 and AgGaGeS_2 [10]. The Ge adding was found to decrease melting temperature from $1050 \text{ }^\circ\text{C}$ for LiGaS_2 to $900 \text{ }^\circ\text{C}$ for $\text{Li}_2\text{Ga}_2\text{GeS}_6$. This lowers a risk of incongruent evaporation when crystal growing. A consequence of such evaporation may be a deviation from the stoichiometric composition and appearing of inclusions of side phases.

In present work large single crystals of $\text{Li}_2\text{Ga}_2\text{GeS}_6$ were grown and their structure and linear optical properties were studied. The shape of the fundamental absorption edge was analyzed and band gap values were estimated. High quality of $\text{Li}_2\text{Ga}_2\text{GeS}_6$ crystals is confirmed by emission of free and self-trapped excitons. These crystals demonstrate an intense photoluminescence which increases about two orders as crystal is cooled to 80 K .

* Corresponding author.

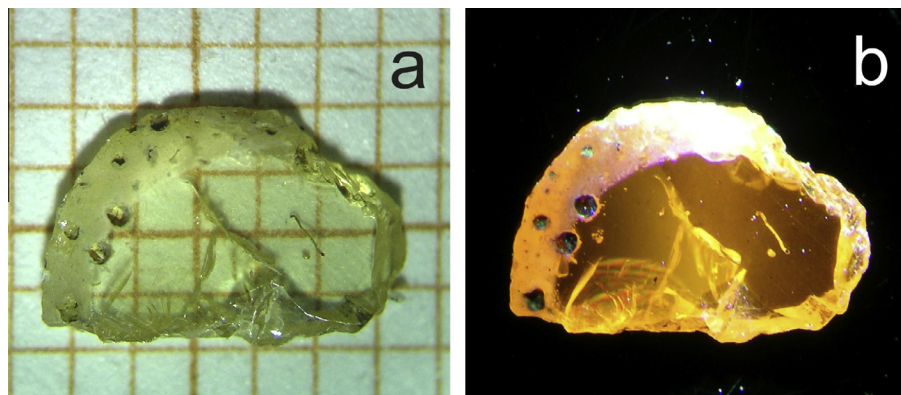


Fig. 1. LGGs plate in reflected light (a) and PL pattern at 365 Hg excitation, at $T = 300$ K (b).

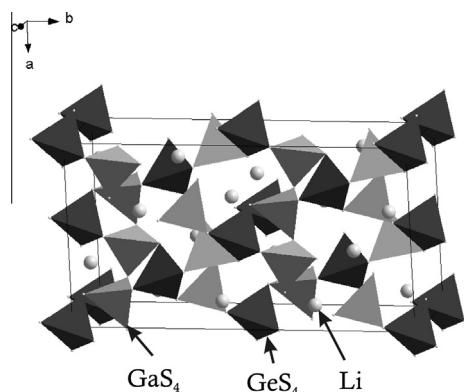


Fig. 2. Crystal structure of $\text{Li}_2\text{Ga}_2\text{GeS}_6$.

2. Experimental

2.1. Crystal growth

Two different furnaces were used for charge synthesis and crystal growth. Crystals of $\text{Li}_2\text{Ga}_2\text{GeS}_6$ were grown in a vertical two-zone furnace by the Bridgman technique. Provisionally synthesized charge was filled into a glass–carbon crucible with a conic bottom, which, in turn, was placed inside a sealed silica ampoule. Ampoule with a crucible was shifted at a rate of 1 mm/day from the upper hot zone (900 °C) to a cold zone (700 °C). Temperature gradient in the crystallization area was about 10 °C/cm.

2.2. X-ray structural analysis

The powder diffraction data of $\text{Li}_2\text{Ga}_2\text{GeS}_6$ for Rietveld analysis were collected at room temperature with a Bruker D8 ADVANCE

Table 1
Main parameters of processing and refinement of the $\text{Li}_2\text{Ga}_2\text{GeS}_6$ sample.

Compound	$\text{Li}_2\text{Ga}_2\text{GeS}_6$
Space group	<i>Fdd2</i>
<i>a</i> (Å)	12.0796 (2)
<i>b</i> (Å)	22.7300 (4)
<i>c</i> (Å)	6.84048 (11)
<i>V</i> (Å ³)	1878.19 (5)
<i>Z</i>	8
2θ -interval (°)	5–110
No. of reflections	329
No. of refined parameters	62
R_{wp} (%)	13.04
R_p (%)	9.49
R_{exp} (%)	8.22
χ^2	1.59
R_B (%)	3.68

powder diffractometer (Cu $K\alpha$ radiation) and linear VANTEC detector. The step size of 2θ was 0.016°, and the counting time was 1.2 s per step. Rietveld refinement was performed by using TOPAS 4.2 [12].

2.3. Optical spectroscopy

Transmission spectra were recorded using a UV-2501 PC Shimadzu spectrometer in the UV to near IR, whereas in the mid-IR we used a Fourier transform spectrometer Infracum 801. The photoluminescence (PL) spectra were measured using a SDL1 luminescence spectrometer with excitation from the 1 kW Xe lamp through the MDR2 monochromator. To record the PL emission we used a cooled FEU83 photomultiplier which is sensitive in the 350–1200 nm range. The photoluminescence excitation (PLE) spectra were corrected to a constant number of incident photons using Na salicylate and Rhodamine 640. Raman spectra were measured using a Horiba Jobin Yvon LabRAM HR800 spectrometer with 1024 pixel LN/CCD detector using the 532-nm Nd:YAG laser. The curves of thermostimulated luminescence (TSL) were recorded when heating crystals at the rate $\beta = dT/dt \sim 20$ °C min^{-1} after UV excitation during 5 min. at 80 K.

3. Results and discussion

3.1. Crystal growth

Compound $\text{Li}_2\text{Ga}_2\text{GeS}_6$ was obtained by pyrosynthesis from elementary 3N lithium, 7N gallium and germanium as well as 5N

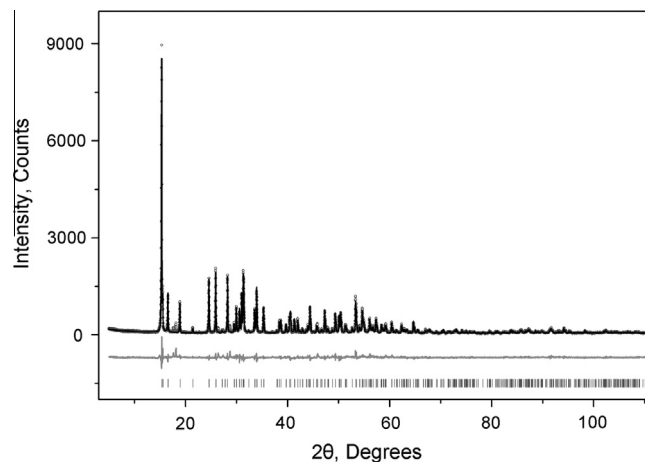


Fig. 3. Difference Rietveld plot of $\text{Li}_2\text{Ga}_2\text{GeS}_6$. Gray circles represent experimental diffraction pattern, black line shows the simulated X-ray pattern, gray line at the bottom shows the difference between experimental and simulated data, sticks at the bottom represent Bragg reflections.

Table 2Fractional atomic coordinates and isotropic displacement parameters (\AA^2) of $\text{Li}_2\text{Ga}_2\text{GeS}_6$.

	x	y	z	B_{iso}
Ge	0	0	0	2.0 (2)
Ga	0.1270 (2)	0.1375 (1)	-0.0321 (5)	1.0 (2)
Li	0.150 (3)	0.061 (2)	0.483 (5)	3.1 (9)
S1	0.0488 (3)	0.0764 (2)	0.1889 (7)	2.0 (2)
S2	0.3058 (4)	0.1190 (2)	-0.0808 (8)	2.0 (2)
S3	0.0965 (3)	0.2292 (3)	0.0678 (8)	2.0 (2)

sulfur. All components taken in a stoichiometric ratio were placed into glasscarbon crucible located inside a silica container. This container was sealed after evacuation and mounted in the two-zone furnace so that lower part of container is located in a hot zone with temperature $T \sim 1000$ °C whereas its upper part is in the cold zone (400 °C). Synthesis time was 5–6 h, afterwards the furnace was switched off. One extracted container after furnace cooling to room temperature. Obtained charge was then displaced into glasscarbon crucible with a conic bottom and a press cap. This crucible was placed into a silica ampoule, evacuated and sealed. Ampoule with the crucible was moved in the furnace at a rate of 1 mm/day from upper hot zone with $T = 900$ °C to the lower cold one (700 °C). Temperature gradient in the crystallization area was 10 °C/cm. Thus, we obtained a $\text{Li}_2\text{Ga}_2\text{GeS}_6$ single crystal about $5 \times 5 \times 10$ mm³ in size. Polished plate, about 1 mm thick, cut from this sample is shown in Fig. 1a. This crystal was of optical quality, slightly yellowish color and demonstrated an intense orange luminescence at UV excitation 365 nm (Fig. 1b).

3.2. Crystal structure

Almost all peaks were indexed by orthorhombic cell (*Fdd2*) with parameters close to $\text{Li}_2\text{Ga}_2\text{GeS}_6$ [10], the structure of which was solved from single crystal (Fig. 2). Therefore this crystal structure was taken as starting model for Rietveld refinement. Refinement was stable and gives low R-factors (Table 1, Fig. 3). Coordinates of atoms and main bond lengths are in Tables 2 and 3 respectively.

$\text{Li}_2\text{Ga}_2\text{GeS}_6$ crystallizes in the orthorhombic space group *Fdd2* with the asymmetric unit containing one crystallographically independent Li atom at the Wyckoff position 16b with 100% occupancy, one independent Ga atom at the Wyckoff position 16b, one independent Ge atom at the Wyckoff position 8a, and three independent S atoms at the Wyckoff position 16b, leading to $\text{Li}_2\text{Ga}_2\text{GeS}_6$ stoichiometry. $\text{Li}_2\text{Ga}_2\text{GeS}_6$ also has a three-dimensional framework built up from corner-sharing LiS_4 , GaS_4 , and GeS_4 tetrahedra (Fig. 2). Here GeS_4 tetrahedra are isolated and are connected by four GaS_4 tetrahedra (Fig. 2) to form the 3D framework. The GeS_4 tetrahedra are formed by two S3 and two S1 atoms. Each S3 corner atom of each GeS_4 tetrahedron is shared by one GaS_4 and two LiS_4 tetrahedra, whereas each S1 is part of one GeS_4 tetrahedron and one LiS_4 tetrahedron. The GaS_4 tetrahedra form an infinite chain by corner sharing of the two S2 atoms; two different chains exist in the *ac* plane forming an acute angle with each other and are cross connected by GeS_4 tetrahedra (Fig. 2). The Li atoms in distorted

Table 3Main bond lengths (\AA) of $\text{Li}_2\text{Ga}_2\text{GeS}_6$.

Ge–S1	2.243 (5)	Ga–S3	2.224 (7)
Ge–S3 ⁱ	2.283 (5)	Li–S1	2.38 (4)
Ga–S1	2.260 (6)	Li–S2 ⁱⁱⁱ	2.34 (4)
Ga–S2	2.226 (5)	Li–S3 ^{iv}	2.95 (4)
Ga–S2 ⁱⁱ	2.222 (6)	Li–S3 ^v	2.79 (3)

Symmetry codes: (i) $-x + 1/4, y - 1/4, z - 1/4$; (ii) $x - 1/4, -y + 1/4, z - 1/4$; (iii) $x - 1/4, -y + 1/4, z + 3/4$; (iv) $-x + 1/4, y - 1/4, z + 3/4$; (v) $x + 1/4, -y + 1/4, z + 1/4$.

tetrahedral coordination form an infinite chain parallel to the *c*-axis and perpendicular to the *a*–*b* plane by corner sharing of the S3 atoms (Fig. 2). The interatomic distances and angles for $\text{Li}_2\text{Ga}_2\text{GeS}_6$ are listed in Table 3. The bond lengths of the main group elements with sulfur are similar to those observed in AgGaGeS_4 [4].

This structure differs from that of LiGaS_2 , where Li or Ga cations occupy half of the tetrahedral holes and all the octahedral interstices are empty. We observed earlier feature in the LiGaS_2 structure [13]: the tetrahedral interstice size of this orthorhombic structure is smaller than that of the Li^{+1} cation, which results in a distortion of the LiS_4 (LiSe_4) tetrahedron accompanied by an increase of the inter-anion distance in one anion pair and its decrease in the others. Such distortion leads to an increase of the Li coordination number from 4 to 5 ($[\text{LiX}_4]-[\text{LiX}_4]\text{X}$) in the first approximation of XDiviMIN tiling.

3.3. Raman spectrum

The Raman spectrum, recorded at 300 K for $\text{Li}_2\text{Ga}_2\text{GeS}_6$ (a) and LiGaS_2 , AgGaS_2 (b) for comparison are given in Fig. 4. Both for LiGaS_2 and LiInS_2 the group-theory analysis shows that at the zone center for the $\beta\text{-NaFeO}_2$ structure, the 48 normal phonon modes are distributed among various irreducible representations of the C_{2v}^9 factor group as follows: $\Gamma^{\text{vib}} = 12A_1 + 12A_2 + 12B_1 + 12B_2$ [7,14]. The three acoustic phonon modes have A_1 , B_1 and B_2 symmetries; the 45 remaining (optical) modes are Raman active. IR absorption spectrum given for $\text{Li}_2\text{Ga}_2\text{GeS}_6$ in [10] was recorded at wavenumbers $\nu > 200$ cm⁻¹ and there was a broad band in the 200–500 cm⁻¹ range with a slightly pronounced structure. Raman spectrum of $\text{Li}_2\text{Ga}_2\text{GeS}_6$ given in Fig. 4 demonstrates a well resolved fine structure in the 50–450 cm⁻¹ range which confirms high quality of the samples. One can see three main groups of peaks in the 50–150, 250–350 and 350–500 cm⁻¹ ranges. Owing to the respective mass of the atoms, the highest-frequency modes obviously imply the movements of Li–S bonds. Phonons of medium frequency (250–350 cm⁻¹) with two dominating lines at 263 and 298 cm⁻¹, visible in both IR-absorption [10] and Raman scattering, are attributed to Ge–S and Ga–S bonds. The phonons of highest frequency (above 350 cm⁻¹) that give rise to strong IR bands but are not observable in Raman spectra are due to weaker Li–S bonds. For AgGaS_2 with a considerably heavier Me^I these modes are shifted to low frequencies. Larger energies for Me^I-C^{VI} vibrations in Li-containing ternary compounds in comparison with AgGaS_2 with chalcopyrite structure favor

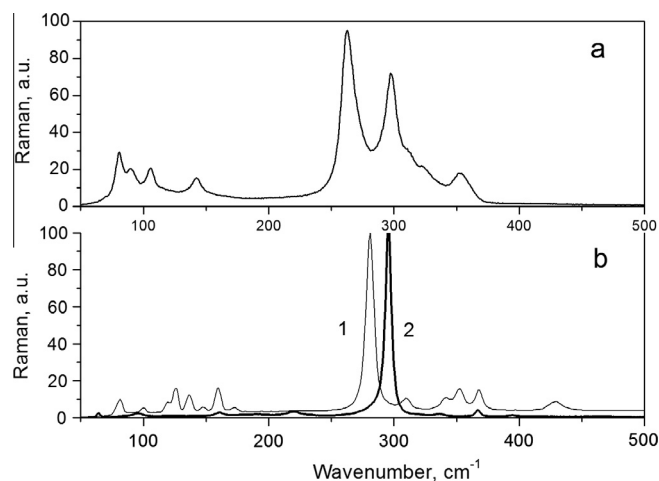


Fig. 4. Raman spectrum for $\text{Li}_2\text{Ga}_2\text{GeS}_6$ (a), LiGaS_2 (b, curve 1) and AgGaS_2 (b, curve 2) recorded at 532 nm excitation. $T = 300$ K.

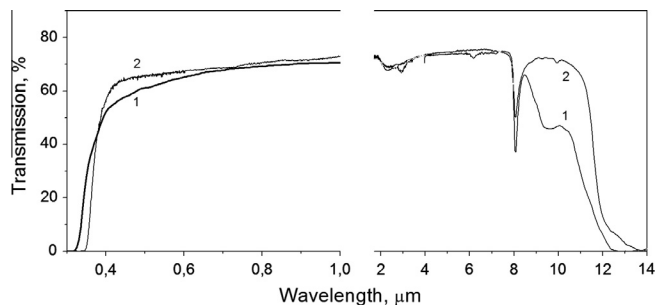


Fig. 5. Transmission spectrum for LiGaS₂ (1) and Li₂Ga₂GeS₆ (2) polished plates 1 mm thick. $T = 300$ K. LiGaS₂ has been annealed in S vapor after growth to reach maximum transparency.

heat dissipation; hence, a higher thermal conductivity is expected for Li₂Ga₂GeS₆; it is expected to be of about $6.0 \text{ Wm}^{-1} \text{ K}^{-1}$ which is ~ 5 times higher than that of AgGaS₂.

3.4. Transmission spectra

In Fig. 5 transmission spectra for 1 mm thick polished plates of Li₂Ga₂GeS₆ and LiGaS₂ are given. LiGaS₂ crystal was annealed in sulfur vapor after growth with allowed one to improve transparency in the working range [15]. Transparency range is 0.33–12.1 μm for LiGaS₂ and 0.355–12.7 μm for Li₂Ga₂GeS₆ on the 5% transmission level. One can see that Transparency range is shifted slightly to longer wavelengths in Li₂Ga₂GeS₆ in comparison with LiGaS₂.

In Fig. 6a fragments of Li₂Ga₂GeS₆ transmission spectra at short waves, recorded at 300 and 80 K are given. Fundamental absorption edge shifts from 353.2 nm to 330.5 nm (on the 5% level) as sample is cooled to 80 K. In Fig. 6b we present the so called Tauc's plot of $(\alpha h\nu)^n$ vs photon energy ($h\nu$) in the region near the fundamental absorption edge, where α is the absorption coefficient calculated from the transmission. The index of power for the Tauc plot is chosen as $n = 2$ in supposition that the edge of fundamental absorption region is determined by the allowed direct electronic transitions [16]. The interpolation of the linear part of curve to zero allows one to estimate the optical band gap of the crystal. Calculated band gap values E_g are 3.51 and 3.72 eV for 300 and 80 K, respectively. Obtained positions of the fundamental transmission edge and band gap values for Li₂Ga₂GeS₆ single crystal are similar to those for a pellet pressed from 3 mg of Li₂Ga₂GeS₆ fine-grained powder members of the with 100 mg of KBr (340 nm and 3.65 eV at 300 K, respectively) [10]. For crystals of

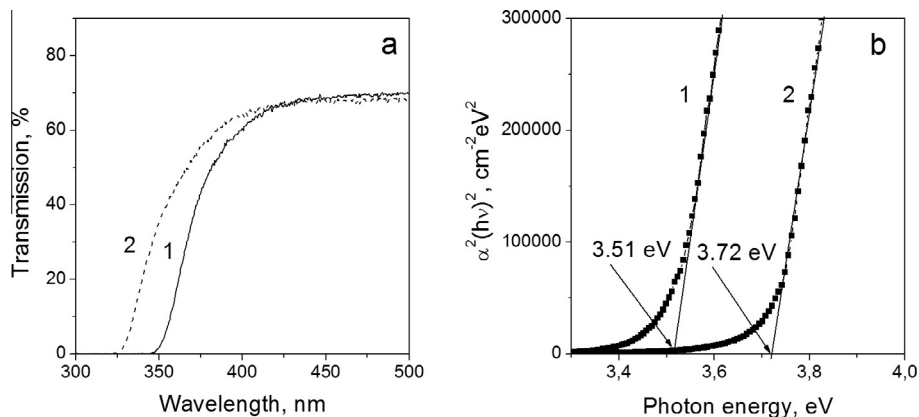


Fig. 6. (a) Fundamental absorption edge in Li₂Ga₂GeS₆ at 300 K (1) and 80 K (2). (b): Absorption edge in Li₂Ga₂GeS₆ at 300 K (1) and 80 K (2), represented in Tauc's coordinates $(\alpha h\nu)^2 = f(h\nu)$: the case of directed allowed electronic transitions. Band gaps are 3.51 and 3.72 eV at 300 and 80 K, respectively.

the LiBC₂ family band gaps values are 3.57 eV for LiInS₂, 2.9 eV (LiInSe₂) [17], 3.34 eV (LiGaSe₂, [9]) and 2.3 eV (LiGaTe₂, [9]) at 300 K. The type of band-to-band transitions in Li₂Ga₂GeS₆ coincides to that for members of the LiBC₂ family [9,17].

In the mid-IR spectral range there is an intense absorption band at 8.0 μm in Li₂Ga₂GeS₆ transmission spectra (Fig. 5): it is similar to that for LiGaS₂ crystals which were annealed in Ga₂S₃ or S₂ vapors [15]. Such band has been observed earlier in the chalcogenide glasses [18]. In LiGaS₂ this band was associated with the S–S vibrations with participation of S in regular sites and adjacent interstitial sulfur ions. A weak absorption band is observed also in the 2–4 μm range. In LiBC₂ crystals position of the long wave transparency edge is determined by 2-phonon and 3-phonon vibrations which take place at wavelength longer than 10 and 7 μm, respectively. Basing on our experience on growing and modification of LiBC₂ crystals [7–9,17] we expect that it may be possible to control transparency by an aftergrowth annealing Li₂Ga₂GeS₆ crystals in proper atmosphere. Taking into account a much lower absorption in the 8–12 μm range in Li₂Ga₂GeS₆ its transparency can be improved considerable particularly in samples of stoichiometric composition.

3.5. Luminescence spectra

In Fig. 7 photoluminescence spectra for Li₂Ga₂GeS₆ recorded at UV 355 nm excitation at 80 K (curve 1) and 300 K (2). There are three dominating broad bands with maximums near 596, 730 and 906 nm as well as a weaker band at 450 nm. At room temperature these samples demonstrate an intense enough orange PL (Fig. 1) however main emission is concentrated in the near IR and it is invisible at visual examination (Fig. 7, curve 2). As temperature lowers to 80 K PL in the 596 nm band increases about two orders and an additional narrow line appears at 371 nm. This line is close to fundamental absorption edge of Li₂Ga₂GeS₆ (333 nm, $E_g = 3.72$ eV in Fig. 6a and b) and may be related to free excitons recombination. As a rule, presence of excitonic lines testifies high quality of the crystals and low concentration of point defects. Broad PL bands are Gaussians and the results of PL spectrum (2) decomposition into four individual components are given in Table 4. FWHM is a full width at half-maximum given in (eV). In Fig. 8 the photoluminescence excitation spectra (PLE) for PL emissions 596, 700, 730 and 950 nm are given. It is obvious that PL in the 596 and 730 nm bands is excited in a broad 370 nm band located in the transparency range, near the fundamental absorption edge. Absorption in the 370 nm band is weak enough and we do not see this band in the transmission spectra (Fig. 5, curve

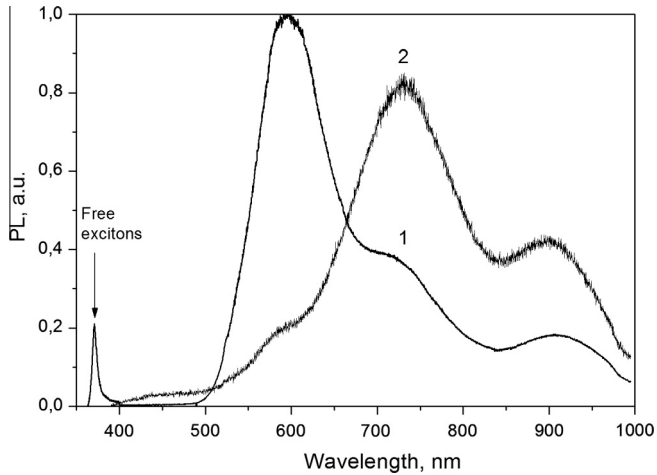


Fig. 7. Photoluminescence spectra for $\text{Li}_2\text{Ga}_2\text{GeS}_6$, recorded at 355 nm excitation at 80 K (1) and 300 K (2). The intensity of spectrum (2) is multiplied by factor of 20.

2). PL 906 nm appears at band-to-band excitation although there is a weaker component in the PLE spectrum near 410 nm. The Stokes shift for 596, 730 and 906 nm PL emissions is large: 1.2, 1.6 and 2.34 eV, respectively.

In Fig. 9 temperature dependences for dominating PL emission are given. One can see that PL quenches quickly in the 80–250 K range as temperature grows. This quenching fits the Mott's law suggested for a model with two recombination channels: one of them is radiative whereas another is nonradiative transition from the relaxed excited state [19]. Temperature dependence of the quantum yield η is described by the following expression:

$$\eta(T) \sim [1 + \tau_R \nu_0 \exp(-\Delta E/kT)]^{-1}, \quad (1)$$

where τ_R is the radiative lifetime at low temperature, ΔE is the energy barrier to the nonradiative decay route, and ν_0 is a jump frequency. The proportional sign is used because other nonradiative decay channels must be available before the system reaches the relaxed excited state. The experimental points in Fig. 9 fit Eq. (1) with ΔE and pre-exponential factors ($\tau_R \nu_0$) with values given in Table 5. All three curves in Fig. 9 demonstrate fast PL quenching as temperature increases in the 80–250 K range, with $\Delta E \sim 0.1$ eV. A two-stage quenching process was observed for 700 nm PL (curve 2).

Taking into account that PL emissions 596, 730 and 906 nm are excited only by the short-wave light (band-to-band or 370 nm band excitation) (Fig. 8), have a large Stokes shift and fast temperature quenching in the 80–200 K range, they all can be associated with recombination of self-trapped excitons [20] located near different defects in the $\text{Li}_2\text{Ga}_2\text{GeS}_6$ lattice. Typical defects may be vacancies, interstitials and cation antisite defects such Ga_{Li} , Ge_{Li} , Ga_{Ge} , Ge_{Ga} and their study is in progress.

In the insert in Fig. 9 a spontaneous emission versus time (or temperature) is shown. It takes place when $\text{Li}_2\text{Ga}_2\text{GeS}_6$ crystal is cooled or heated in the 80 to 170 K range at the rate $\beta = dT/dt$ of about 20 K/min. Such emission occurs in the darkness, without

Table 4
Parameters of Gauss components in the PL spectra for $\text{Li}_2\text{Ga}_2\text{GeS}_6$.

NN	Max position (nm)	Max position (eV)	FWHM (eV)
1	906	1.368	0.19
2	730	1.698	0.339
3	596	2.08	0.448
4	451	2.75	0.464
5	371	3.341	0.061

any excitation: it is typical only of pyroelectrics and is a result of the modification in atomic polarization in crystal volume as temperature changes [21]. The strength of accumulated pyroelectric field can reach many tens of kV. The occurrence of such pyroelectric luminescence (PEL) in $\text{Li}_2\text{Ga}_2\text{GeS}_6$ indicates that there is no symmetry center in the lattice. This agrees with the orthorhombic cell $Fdd2$ as it has been established in Section 3.2. Spontaneous light flashes are a result of the electric break-down and they happen both on crystal surface and inside it [21]. We have also observed the PEL effect in many typical nonlinear optical crystals such as LiIO_3 , $\beta\text{-BaB}_2\text{O}_4$ (BBO), LiB_3O_5 (LBO), Ag_3AsS_3 , LiNbO_3 , LiGaS_2 , and KTP [21]. PEL disappearance at high temperature may be a result of electrical conductivity increase as temperature grows: increased conductivity promotes the leak of the pyroelectric charge and the break-down probability becomes smaller. PEL effect shows a low electrical conductivity of $\text{Li}_2\text{Ga}_2\text{GeS}_6$ samples and in turn a low concentration of electrically active defects. Increase of defect concentration also results in a leak of pyroelectric charge and PEL quenching.

In Fig. 10 one can see a curve of thermostimulated luminescence for $\text{Li}_2\text{Ga}_2\text{GeS}_6$ after 355 nm excitation and the results of decomposition of this TSL curve into individual components. There are four well-pronounced peaks with maximums at 106, 149, 269 and 368 K. Signal rise at $T > 450$ K is associated with a

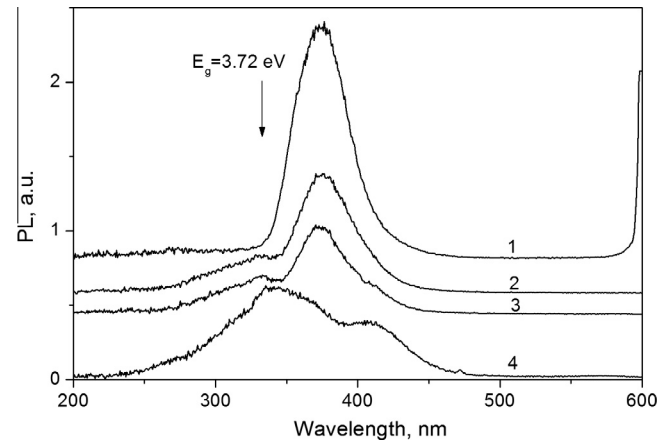


Fig. 8. Luminescence excitation spectra for $\text{Li}_2\text{Ga}_2\text{GeS}_6$ for 600 (1), 700 (2), 750 (3) and 940 nm (4) emissions, at 80 K. An arrow shows band gap at 80 K.

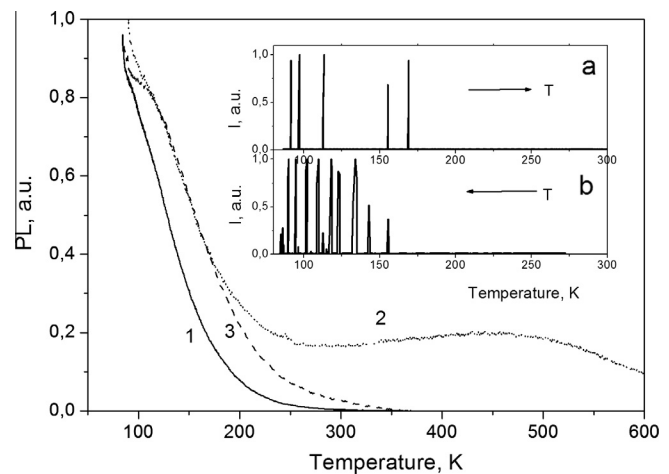


Fig. 9. Temperature dependence for 580 (1), 700 (2) and 950 nm (3) emissions in $\text{Li}_2\text{Ga}_2\text{GeS}_6$ crystal, at 355 nm excitation. In the insets: spontaneous pyroelectric luminescence at heating (a) and cooling (b).

Table 5
Parameters of the Mott law fitting in the PL temperature dependence for $\text{Li}_2\text{Ga}_2\text{GeS}_6$.

PL band maximum (nm)	Pre-exponential factor $\tau_R\nu_0$	Thermal activation energy ΔE (eV)
580	$1.5 \cdot 10^3$	0.085
700	$8 \cdot 10^3$	0.12
	$2.5 \cdot 10^3$	0.63
900	$1.2 \cdot 10^3$	0.10

Table 6
Results of TSL simulation in $\text{Li}_2\text{Ga}_2\text{GeS}_6$: Parameters of individual TSL peaks.

NN	Peak position (K)	Half-width at low temperatures, $\delta 1$ (K)	Half-width at high temperatures, $\delta 2$ (K)	Escape factor (sec^{-1})	Thermal activation energy, E_T (eV)
1	106.0	13.8	16.0	$2 \cdot 10^3$	0.105
2	149.2	17.4	20	$2 \cdot 10^3$	0.152
3	269.2	19.0	22.4	$7 \cdot 10^3$	0.520
4	398.0	38.3	45.5	$5 \cdot 10^4$	0.540

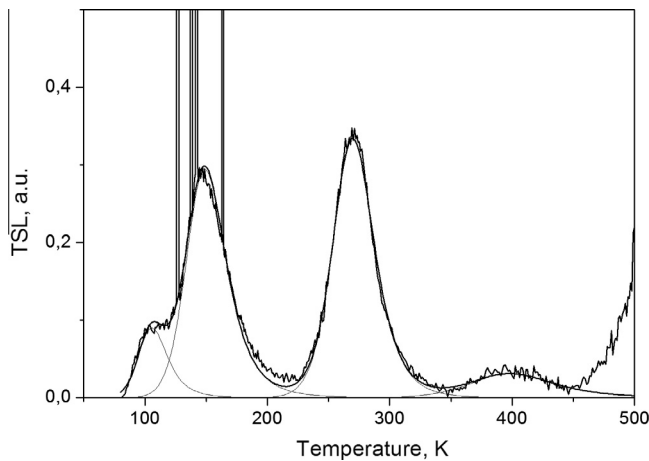


Fig. 10. TSL curves with PEL flashes in the 80–170 K range recorded for $\text{Li}_2\text{Ga}_2\text{GeS}_6$ crystal after 355 nm excitation at 80 K. Thin solid lines show individual TSL peaks: it is a result of TSL curve decomposition following Eq. (2). A smooth curve shown by a thick solid line is a sum of four individual peaks with parameters given in Table 6.

heater glow. Analysis of the peaks shape shows that they are symmetric enough and half-width at half-maximum (HWHM) values at rise and at decay ($\delta 1$ and $\delta 2$, respectively) are close enough and sometimes $\delta 2 > \delta 1$. This indicates a second order of TSL kinetics when probability of recombination of free carriers is negligible compared with the probability of their retrapping [22]. A shape of TSL peak is described by the following expression [22]:

$$I(T) = n_0^2 s \exp(E_T/kT) / \left[1 + (n_0 s / \beta) \times \int_{T_0}^T \exp(-E_T/kT) dT \right]^2, \quad (2)$$

where n_0 is the initial concentration of electrons, s is the escape factor, β is the rate of linear heating (K min^{-1}), k is the Boltzmann's constant, E_T is the thermal activation energy (eV) and T_0 is the initial temperature [22]. There is a good coincidence between experimental data and calculation results (Fig. 10). There are also PEL flashes in the 120–170 K range, but temperature range where PEL occur, their frequency and intensity are smaller than in Fig. 9 (in the case when PEL is observed without preliminary excitation at low temperature). Such PEL weakening is due to an increase in electrical conductivity at charge carriers release from traps and a partial leak of pyroelectric charge.

One can notice that two low-temperature TSL peaks at 106 and 149 K in Fig. 10 are located just in the range of fast temperature quenching for PL emissions 596, 730 and 906 nm. Thus, these TSL peaks can be ascribed to the thermal release of self-trapped charge carriers which are localized components of the self-trapped excitons.

This moment the field of $\text{Li}_2\text{Ga}_2\text{GeS}_6$ application is nonlinear optics: a conversion of laser frequency and generation of coherent radiation in the mid-IR. Because of strong temperature quenching and low PL intensity at room temperature it is difficult to consider $\text{Li}_2\text{Ga}_2\text{GeS}_6$ promising as a conventional scintillator. However lithium presence in their structure makes possible $\text{Li}_2\text{Ga}_2\text{GeS}_6$ usage also as a low-temperature scintillator or working material of semiconducting detector of neutrons or solar axions because of their high interaction cross-section with Li [23]. For such applications $\text{Li}_2\text{Ga}_2\text{GeS}_6$ should be enriched in ^6Li .

4. Conclusions

- Large $\text{Li}_2\text{Ga}_2\text{GeS}_6$ single crystals of optical quality were grown. Their orthorhombic, *Fdd2* structure was confirmed. High crystal quality is confirmed by their well-resolved Raman spectra.
- The shape of fundamental absorption edge is determined by direct allowed electronic transitions: Band gap values were estimated at 80 and 300 K for $\text{Li}_2\text{Ga}_2\text{GeS}_6$. Absorption at 8.0 μm is related to S–S vibrations with participation of interstitial sulfur.
- Features due to free excitons (line 371 nm) and self-trapped excitons (broad 596, 730 and 906 nm bands) were revealed in PL spectra for $\text{Li}_2\text{Ga}_2\text{GeS}_6$.
- Fast temperature quenching of $\text{Li}_2\text{Ga}_2\text{GeS}_6$ luminescence was found. Parameters of PL quenching were calculated in the Mott model. Parameters of four traps of charge carriers dominating in TSL curves were estimated.
- Pyroelectric luminescence was found in $\text{Li}_2\text{Ga}_2\text{GeS}_6$: this confirms the absence of symmetry center in the lattice and $\text{Li}_2\text{Ga}_2\text{GeS}_6$ fitness for nonlinear optics.

Acknowledgements

This work was supported by the Russian Foundation of Basic Research (Grant No. 15-02-03408a).

References

- [1] D.S. Chemla, P.J. Kupecek, D.S. Robertson, R.C. Smith, Silver thiogallate, a new material with potential for IR devices, *Opt. Commun.* 3 (1971) 29–31.
- [2] G.D. Boyd, H.M. Kasper, J.H. McFee, F.G. Storz, Linear and nonlinear properties of some ternary selenides, *IEEE J. Quantum Electron.* 8 (1972) 900–908.
- [3] G.D. Boyd, E. Buehler, F.G. Storz, Linear and nonlinear optical properties of ZnGeP_2 and CdSe , *Appl. Phys. Lett.* 18 (1971) 301–304.
- [4] V.V. Badikov, A.G. Tyulyupa, G.S. Sheverdyayeva, S.G. Sheina, Solid solutions in systems $\text{AgGaS}_2\text{–GeS}_2$, $\text{AgGaSe}_2\text{–GeSe}_2$, *Inorg. Mater.* 27 (1991) 177–185.
- [5] V. Petrov, V. Badikov, G. Sheverdyayeva, V. Chizhikov, Phase-matching properties and optical parametric amplification in single crystal of AgGaGeS_4 , *Opt. Mater.* 26 (2004) 217.
- [6] P.G. Schunemann, Growth of new quaternary nonlinear optical crystals for 1-micron-pumped mid-IR generation, *Proc. SPIE* 6103 (2006) 610303.
- [7] S. Fossier, S. Salaun, J. Mangin, O. Bidault, I. Thenot, J.-J. Zondy, W. Chen, F. Rotermond, V. Petrov, J. Henningsen, A. Yelisseyev, L. Isaenko, S. Lobanov, O. Balachninaite, S. Sleky, V. Sirutkaitis, Optical, vibrational, thermal, damage and phase-matching properties of lithium thioindate, *JOSA B* 21 (2004) 981–2007.
- [8] V. Petrov, J.-J. Zondy, O. Bidault, L. Isaenko, V. Vedenyapin, A. Yelisseyev, W. Chen, A. Tyazhev, S. Lobanov, G. Marchev, D. Kolker, Optical, thermal, electric, damage and phase-matching properties of lithium selenoindate, *JOSA (B)* 27 (N9) (2010) 1902–1927.
- [9] L. Isaenko, A. Yelisseyev, S. Lobanov, P. Krinitsin, V. Petrov, J.-J. Zondy, Ternary chalcogenides LiBC_2 (B = In, Ga; C = S, Se, Te) for mid-IR nonlinear optics, *J. Noncryst. Solids* 352 (2006) 2439–2443.

- [10] Y. Kim, I. Seo, S.W. Martin, J. Baek, P.S. Halasyamani, N. Arumugam, H. Steinfink, Characterization of new IR nonlinear optical materials with high laser damage thresholds, $\text{Li}_2\text{Ga}_2\text{GeS}_6$, *Chem. Mater.* 20 (2008) 6048–6052.
- [11] V. Petrov, A. Yelisseyev, L. Isaenko, S. Lobanov, A. Titov, J.-J. Zondy, Second harmonic generation and optical parametric amplification in the mid-IR with orthorhombic biaxial crystals LiGaS_2 and LiGaSe_2 , *Appl. Phys. B* 78 (2004) 543–546.
- [12] Bruker AXS TOPAS V4, General profile and structure analysis software for powder diffraction data, User's Manual, Bruker AXS, Karlsruhe, Germany, 2008.
- [13] L. Isaenko, I. Vasilyeva, A. Merkulov, A. Yelisseyev, S. Lobanov, *J. Cryst. Growth* 275 (2005) 217–223.
- [14] A.P. Yelisseyev, M.K. Starikova, V.V. Korolev, L.I. Isaenko, S.I. Lobanov, Photoluminescence of lithium thiogallate LiGaS_2 , *JOSA B* 29 (2012) 1003–1011.
- [15] A. Yelisseyev, Z.S. Lin, M. Starikova, L. Isaenko, S. Lobanov, Optical transitions due to native defects in nonlinear optical crystals LiGaS_2 , *J. Appl. Phys.* 111 (113507) (2012) 11.
- [16] D.L. Wood, J. Tauc, Weak absorption tails in amorphous semiconductors, *Phys. Rev. B* 5 (1972) 3144–3151.
- [17] J.-J. Zondy, V. Petrov, A. Yelisseyev, L. Isaenko, S. Lobanov, Orthorhombic crystals of lithium thioindate and selenoindate for nonlinear optics in the mid-IR, in: M. Ebrahimzadeh, I.T. Sorokina (Eds.), *Mid-IR Coherent Sources and Applications*, Springer Verlag, 2007, pp. 67–104.
- [18] V.F. Kokorina, *Glasses for Infrared Optics*, CRC, Boca Raton, FL, 1996, p. 236.
- [19] B. Henderson, G.F. Imbusch, *Optical Spectroscopy of Inorganic Solids*, Clarendon, Oxford, 1989, p. 183.
- [20] K.S. Song, R.T. Williams, *Self-trapped Excitons*, vol. XII, Springer Verlag, Berlin, 1993, p. 403.
- [21] A.P. Yelisseyev, L.I. Isaenko, M.K. Starikova, Optical study of defects in lithium iodate $\alpha\text{-LiIO}_3$, *JOSA B* 29 (2012) 1430–1435.
- [22] S.W.S. McKeever, *Thermoluminescence of Solids*, Cambridge Uni. Press, Cambridge, London, New-York, 1988.
- [23] E. Tupitsyn, P. Bhattacharya, E. Rowe, L. Matei, M. Groza, B. Wiggins, A. Burger, A. Stowe, Single crystal of LiInSe_2 semiconductor for neutron detector, *Appl. Phys. Lett.* 101 (2012) 202101.